Nano Research

Open Access

Research Article

Ultrafast laser high precision patterning on single-crystal diamond toward micro/nano functional devices

Haoze Han[1,2,§], Ming Qiao[1,3,§], Yuzhi Zhao[1,2], Ma Luo[1,2], Jiaqun Li[1,2] ✉, Yunshuo Zhang[1,2], Yuichi Kozawa[4], and Jianfeng Yan[1,2] ✉

[1] *Department of Mechanical Engineering, Tsinghua University, Beijing 100084, China*
[2] *State Key Laboratory of Tribology in Advanced Equipment, Tsinghua University, Beijing 100084, China*
[3] *State Key Laboratory of Precision Manufacturing for Extreme Service Performance, College of Mechanical and Electrical Engineering, Central South University, Changsha 410083, China*
[4] *Institute of Multidisciplinary Research for Advanced Materials, Tohoku University, 2-1-1 Katahira, Aoba-Ku, Sendai 980-8577, Japan*
§ *Haoze Han and Ming Qiao contributed equally to this work.*

Cite this article: *Nano Research*, **2026**, *19*, 94908402. https://doi.org/10.26599/NR.2026.94908402

ABSTRACT: Single-crystal diamond has attracted much attention because of its wide bandgap and specific thermal and optical properties, which is suitable for the utilization on integrated photonic devices and power semiconductor devices. However, its extremely high hardness confines the processing ability of micro/nano structures, which is the main determinant of devices performance. Here, multimode patterning methods using ultrafast laser regulated in spatial-domain with high precision are proposed. Through designing of spatial beam phase, specific patterned micro/nano structures ranging from sub-micrometer scale to millimeter scale can be printed on diamond surface with improved efficiency. This provides a facile strategy for the fabrication of programmable patterns with sub-wavelength resolutions. The laser ablation and graphitization result can be precisely predicted by calculating free electron density and validated through patterning experiment. A diamond holographic element is designed and fabricated through the proposed method, which can project the reconstructed holographic image for display applications. This work presents a promising method for preparing of single-crystal diamond-based next-generation semiconductor devices and integrated photonic systems requiring precise light field control.

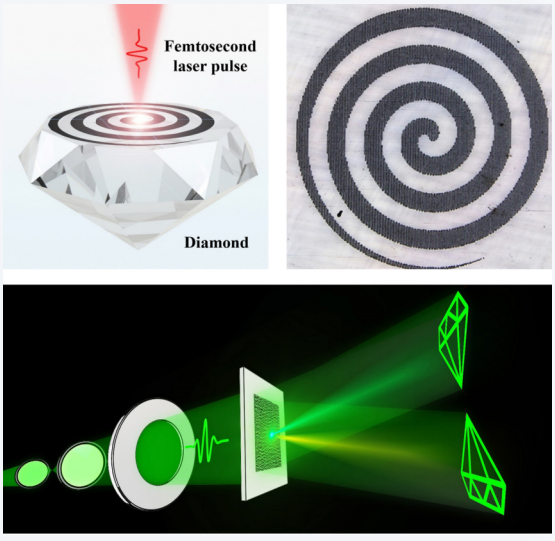

KEYWORDS: ultrafast laser fabrication, high precision, patterned processing, single-crystal diamond, micro/nano functional devices

1 Introduction

Transparent dielectrics and wide bandgap semiconductors are applicable in next-generation micro/nano functional devices owing to their unique physical and chemical properties [1–3]. Single-crystal diamond is considered the most promising next-generation semiconductor material [4], with band gap of 5.47 eV. Due to its exceptional hardness, high thermal conductivity, and broad optical transmission spectrum, it is an attractive material for fabricating power semiconductor devices and optical devices [5–8] with long lifespan, high power-handling capacity, and light transmission performance [9–12]. For instance, a spiral phase plate fabricated by femtosecond laser beam shows the capability to transform laser beams into hollow ring beams and optical vortex beams [13]. Additionally, a two-dimensional photonic crystal slab nanocavity increases spontaneous emission rates and photon extraction efficiencies, facilitating high-efficiency optical information transmission [14].

Recently, laser scribing and inscribing technology has emerged as

Received: October 13, 2025; **Revised:** December 26, 2025
Accepted: December 29, 2025

✉Address correspondence to Jiaqun Li, lijiaqun@mail.tsinghua.edu.cn; Jianfeng Yan, yanjianfeng@tsinghua.edu.cn

a promising technique for glasses and silicon micro-nano processing due to its three-dimensional and mask-free features [15–21]. When using continuous wave lasers or long-pulsed lasers to process these brittle materials, heat accumulation and internal stress induced by excessive energy deposition are inevitable. This leads to micro-crack propagation and lattice damage formation, which is not suitable for optical applications [22, 23]. Specifically, when using continuous-wave or long-pulse lasers (such as nanosecond lasers) to process diamond, significant thermal damage occurs, leading to irreversible graphitization of the sp^3-bonded carbon phase [24, 25]. This method produces a thicker graphitized layer and more extensive heat-affected zone (HAZ). Therefore, it is limited to use long-pulse lasers for precision processing on diamond. Consequently, conventional manufacturing technologies meet limitations when processing micro/nano structures either at the surface or within the material volume of these brittle materials.

Ultrafast lasers represent a potential solution to address the challenges [26, 27]. The ultrashort pulse duration and ultrahigh power density minimize heat affected zones and recast layers, evidently enhancing processing quality [28–31]. However, current scanning methods for micro array impose limitations on the flexibility and efficiency of ultrafast laser processing. Fabrication quality is often compromised due to laser beam overlaps [32], while structure intervals must be maintained at certain distances to prevent secondary processing effects. Therefore, it is necessary to optimize laser high-precision patterning and scanning strategies. To overcome constraints of gaussian beam and improve processing abilities, spatial regulated laser processing methods designed for increased energy efficiency ratio and precision have been developed. Advanced techniques such as multi-beam processing and vortex beam processing, which utilize shaped optical fields, significantly increase fabrication capacity and processing capabilities. Through the integration of advanced optical focusing systems and precise pulse energy control, laser spots can be controlled to hundreds of nanometers, which substantially promotes the processing resolution [33–36]. A multi-dimensional laser nanolithography method using spatial light modulators was proposed to produce non-diffracting beams to induce planar nanopatterns deep inside silicon, enabling creation of nano-voids within the irradiated volumes and fabrication of controlled nanostructures [37]. Similarly, a nanoscale femtosecond laser multi-beam lithography method was proposed to fabricate advanced photonic crystal, achieving sub-wavelength control of structural dimensions without the limitations of conventional single-beam processing approaches [38]. These developments in ultrafast laser spatiotemporal shaping provide methods for manufacturing high-performance diamond-based optical devices, which can be applied in optical communications and photonic systems requiring precise light field control.

In this study, an ultrafast laser facile patterning method was performed to produce structures from sub-micrometer scale to millimeter scale in single-crystal diamond materials, which have potential applications in micro/nano functional devices. The composition change of single-crystal diamond materials under ultrafast laser irradiation was studied. Controllable ablation and graphitization process with tunable precision were investigated by free electron density calculating with plasma model. Using point-by-point scanning method, microstructure arrays for light modulation were produced. When using spatial shaped laser micropatterning method, the processing efficiency can be further increased. Based on the proposed laser micropatterning method, optical diffraction devices designed by Gerchberg–Saxton (GS) algorithm were fabricated on diamond substrates to generate predetermined optical patterns.

2 Results and discussion

2.1 Laser ablation and graphitization on diamond

The composition and structure change through laser irradiation on single-crystal diamond material were summarized and displayed in Fig. 1. As shown in Fig. 1(a), the femtosecond laser beam is focused

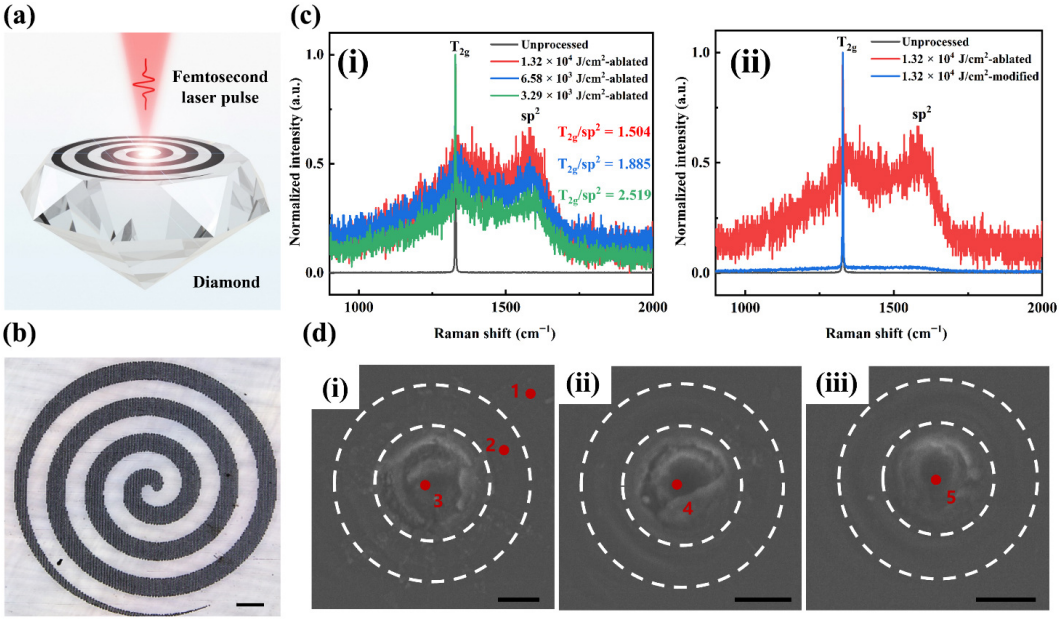

Figure 1 The composition and structure change through laser irradiation on single-crystal diamond material. (a) Schematic of femtosecond laser pulse irradiation on diamond surface for pattern processing. (b) Optical image of spiral phase plates fabricated on diamond surface. (c) Raman result of the spot irradiated by different laser pulse energy, the spectral sampling areas are shown in (d). (d) SEM images of the spot irradiated by different laser pulse energy: (i) 1.32×10^4 J/cm^2, (ii) 6.58×10^3 J/cm^2, and (iii) 3.29×10^3 J/cm^2. (b) Scale bar is 100 μm. (d) Scale bar is 2 μm.

onto the single-crystal diamond material through a focusing objective, and micro patterns are fabricated on the surface. As a result, Fig. 1(b) presents a pattern consisting of thousands of spot structures was produced, where each spot was processed by laser irradiation using single laser pulse. To analyze the surface changes before and after laser irradiation, scanning electron microscope (SEM) imaging and Raman spectroscopy were employed. Figure 1(c) displays the normalized Raman spectra of diamond obtained before and after laser irradiation, sampling the spot structures processed with different pulse energy. The pristine diamond exhibits a characteristic Raman peak (T_{2g} peak) at 1332 cm^{-1} [39], with an intensity ratio $I(T_{2g})$ of approximately 100%. When diamond is irradiated by a single laser pulse with 1.32×10^4 J/cm^2 pulse energy fluence, a characteristic peak approaching graphitization (sp^2 peak) appears at 1579 cm^{-1} in the ablated area, while the typical range of graphitization is between 1580 and 1600 cm^{-1}, indicating a transformation from sp^3 to sp^2 bonding due to the laser pulse energy deposition. It should be noted that, the sp^2 peak intensity in modified areas shows only slight increases, suggesting that graphitization predominantly occurs at the center of beam irradiation rather than along its periphery. As pulse energy fluence increases from 3.29×10^3 to 1.32×10^4 J/cm^2, the ratio of intensities $I(T_{2g})/I(sp^2)$ decreases from 2.519 to 1.504, indicating more extensive graphitization. The degree of graphitization with different laser energy shows that the more laser energy is deposited, the more intense the transformation of the diamond material structure caused. Figure 1(d) presents a SEM image of the processed spot structure with different laser parameters. The fabricated spot structure exhibits a concentric circle, where Region 1 corresponds to the unprocessed area composed of pristine diamond, Region 2 represents the modified area after laser irradiation with pulse energy fluence of 1.32×10^4 J/cm^2. Regions 3, 4, and 5 correspond to ablated areas after laser irradiation with pulse energy fluences of 1.32×10^4, 6.58×10^3, and 3.29×10^3 J/cm^2, respectively. This concentric pattern results from the Gaussian profile of the laser beam, which exhibits maximum energy intensity at the center and decreases radially toward the periphery. The spatial energy distribution creates distinct processing zones, indicating the existence of specific fluence thresholds separating ablation and modification. In the ablated region, material removal results in the formation of crater-like structures, with periodic nanostructures observed at the bottom of these craters. In the surrounding modified region, the phase transition from sp^3 to sp^2 bonding and the refractive index of the material changes, where no bump-like structures or crater-like structures are formed in this area.

Free electron density is a crucial parameter for determining the ablation threshold of diamond, and it can be calculated through plasma model, considering collisional ionization, photonic ionization, and localized transient optical properties. In order to study the relationship between free electron density and the ablation threshold of diamond, some simulation and experiments were employed. A series of parametric experiments were performed to determine the laser energy fluence range. By varying the laser energy, the morphology processed by single pulse transitioned from exhibiting an ablation crater and modified ring, to only a modified zone, and finally to no visible processed traces. Figure 2(a) illustrates the different regions fabricated on the diamond surface using femtosecond laser pulses by a focusing objective (10×, numerical aperture (NA) = 0.3). According to the SEM results shown in Fig. 1(d), the surface exhibits two distinct regions: The inter region is an ablation zone and the outer region is a modification zone. Figure 2(b) shows the optical images of the diamond surface after femtosecond laser irradiation using double-pulse femtosecond laser. Double-pulse laser processing can be utilized to determine the free-electron relaxation time of materials, by varying the pulse delays and single pulse energy of two laser pulses with identical energy. The clear boundaries are evident between the ablation, modification and unprocessed zones, which correspond to the ablation threshold and modification threshold. In the ablation zone, dark central craters are observed at the laser irradiation center, surrounded by bright modified regions; in the modification zone, only bright circular areas are present. Experimental data show that as the double-pulse delay time increases from 0 to 900 fs, the surface ablation threshold gradually increases. This continuous increase in ablation threshold could be attributed to temporal regulation of electron–phonon interactions. Longer delays allow more electron energy transfer to the lattice, which induce the decrease of the peak intensity of free electron density, resulting in higher input fluence required for material ablation. Theoretically, material ablation occurs when the free electron density equals or exceeds the critical electron density, and the calculated critical electron density was determined to be 1.75×10^{21} cm^{-3} when the laser wavelength was 800 nm. The free electron relaxation time of single-crystal diamond was determined to be about 600 fs according to the ablation results. Figure 2(c) illustrates the free electron density as a function of various laser fluence values according to the plasma model. This analysis reveals that at 20 J/cm^2, the electron density remains below the critical electron density, whereas at 40 J/cm^2, it exceeds the ablation threshold. These observations indicate that the ablation fluence threshold lies within the interval between 20 and 40 J/cm^2. To determine this threshold with precision, the relationship between the laser energy fluences and the diameters of the ablation or modified areas is established in Fig. 2(d), through measuring the size of processed spots on diamond under different laser energy. There exists a linear relationship between the square of the circle diameter after laser irradiation and the logarithm of laser pulse fluence. When the diameter of the processed area exceeds zero, the corresponding laser energy fluence represents the threshold value. By applying this approach, an ablation threshold of 36.41 J/cm^2 and modification threshold of 14.88 J/cm^2 were identified, which provides a more accurate determination of the threshold value through systematic diameter measurements across varying fluence levels. It is worth mentioning that the processing threshold of the material is affected by factors such as laser wavelength, laser pulse width, and focusing conditions, so the obtained threshold is applicable to specific processing situations. As shown in Fig. 2(e), the peak intensity of free electron density with pulse energy fluence of 36.41 J/cm^2 exceeded the critical electron density, and the single crystal diamond material would begin to be ablated. Thus, the regulation of ultrafast laser provides more dimensions to control the precision of micro/nano structures.

2.2 Vortex structure fabrication with point-by-point strategy on large format

After the processing energy fluence threshold of single-crystal diamond is determined, different laser energy can be chosen to process hole structures point-by-point on the diamond surface. The micro-hole structures exhibit a different refractive index compared

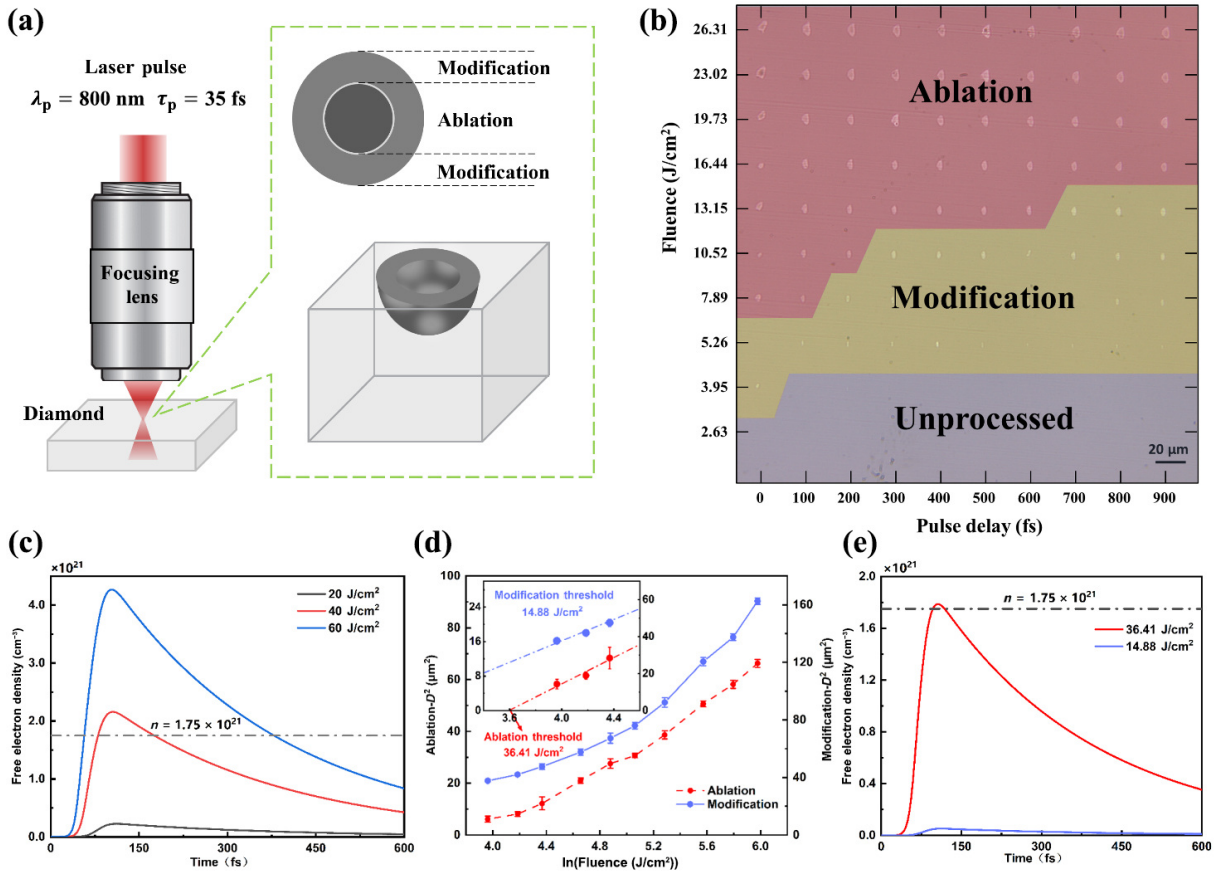

Figure 2 The experimental and simulation results of fabrication threshold of diamond. (a) Schematic of different areas fabricated by ultrafast laser pulse on diamond. (b) Optical image of the double laser pulse fabrication result, scale bar: 20 μm. (c) Calculated free electron density with different laser pulse fluence. (d) The square of diameter of ablation or modification areas as a function of logarithm of laser pulse fluence. The inset shows a magnified view of the region where the vertical axis value in (d) approaches zero. (e) Calculated electron density with experimental ablation and modification fluence.

to the surrounding areas, which enables a splicing of large format structures. Based on the principle of light diffraction, the phase of the light beam passing through the component is modulated, thereby generating an output optical field with a specific shape. Using a point-by-point scanning method, designed patterns composed of ablated spots can be written on the diamond material, and these micro patterns can control light propagation through the structure. Figure 3 primarily shows the patterning capability of the point-by-point scanning method and the phase plate design methodology. As presented in Fig. 3(a), spiral phase plates (SPPs) with different topological charges (1, 2, and 3, respectively) can be fabricated by a focusing objective (20×, NA = 0.45) using this laser point-by-point ablation technique. The topological charge characterizes the magnitude of the orbital angular momentum of a vortex beam, which can influence the shape of the output optical field [8]. The corresponding detailed structures are shown in Fig. 3(b), which shows the micro patterns are composed of spots with the same size. When an 800 nm laser beam propagates through these SPP patterns, the wavefront undergoes phase modulation resulting in distinctly shaped light fields. Figure 3(c) presents simulation results of light fields shaped by SPPs with different topological charges, showing how these diamond surface patterns control the optical field distribution. The fabricated SPPs with varying topological charges exhibit designed optical properties, confirming light phase modulation. Moreover, increasing pattern complexity enables the generation of correspondingly more complexed light field distributions, suggesting potential applications in optical manipulation and information dissemination.

2.3 Micro-nano structure fabrication using shaped laser beam

To improve the efficiency of diamond surface patterning beyond point-by-point scanning methods, structured light fields can be employed to process micro-nano patterns through single laser pulse irradiation. This approach utilizes femtosecond pulsed laser beams in combination with a spatial light modulator (SLM) to directly write patterned structures on diamond surfaces with single laser pulse, which enables beam shaping through uploaded holograms on SLM. During processing, material removal occurs in regions where the intensity exceeds the material's ablation threshold, while lower-intensity regions remain unaffected. Consequently, the resulting ablation patterns closely correspond to the intensity distribution of the shaped beam, enabling rapid fabrication of complex micro-nano structures using single laser pulse. This method can be extended to other transparent materials, and experimental determination of optimal laser energy parameters for different materials is required.

The relationship between SLM holograms, the resulting light field distributions, and the corresponding processed structures on diamond was shown in Fig. 4. As presented in Fig. 4(a), when a vortex phase with topological charge n = 3 is applied to the SLM, the output beam forms a circular vortex light field. Through

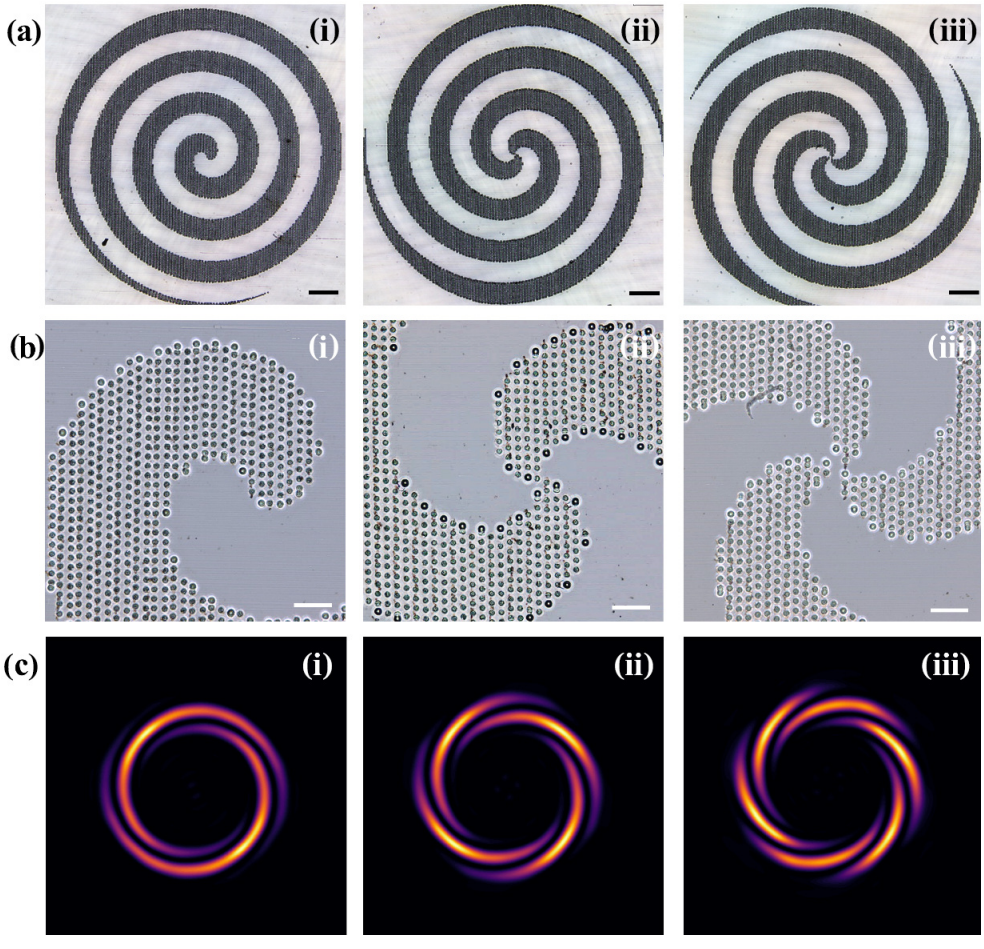

Figure 3 Optical images and interference patterns of spiral phase plates with different topological charges. (a) Optical images of SPPs with different topological charges inscribed by ultrafast laser, scale bar is 100 μm. (b)(i)–(b)(iii) Detailed optical images correspond to the ablated areas in the center of areas in (a)(i)–(a)(iii), scale bar is 20 μm. (c) Simulation results of the optical field irradiated through the micro patterns by Gaussian beam.

interaction between laser pulse and diamond material, this shaped beam with a single-pulse energy of 50 μJ, which is focused by an objective lens (50×, NA = 0.5), produces a corresponding circular ring structure on the diamond surface. Figure 4(b) shows a higher-order Bessel phase, which combines an ordinary Bessel phase with a vortex phase with topological charge n = 3. This phase configuration generates a circular vortex field with increased non-diffraction propagation distance, resulting in larger toroidal structures after focused processing compared to those in Fig. 4(a). Besides the circular patterns, the SLM can generate split-beam light fields for parallel processing. Figures 4(c) and 4(d) present four-petal and six-petal beam patterns respectively, enabling simultaneous ablation of multiple spots on the diamond surface. The overall morphology of the processed patterns is consistent with the shaped light field. Beam quality may affect the symmetry of the fabricated structures. The size of the processed points was about 650 and 500 nm, which is subwavelength (800 nm) and sufficient for the fabrication of a wide range of functional diffractive devices. Additionally, this method can effectively control the spatial distribution of ablation features and improve the efficiency of micropatterning. By using a N-beam shaped light field, the efficiency of micropatterning fabrication process can be raised by N−1 times. Thus, the efficiency was raised by 3–5 times using shaped light field shown in Figs. 4(c) and 4(d). The experimental results in Fig. 4(e) show that combining a six-petal phase with a Bessel phase preserves the six-petal light field configuration while increasing the distance between each petal and the central point from 1 to 2 μm, showing spatial tunability of the fabricated microstructures. By optimizing the phase algorithm and incorporating aberration correction techniques, it is promising to achieve higher processing accuracy and smaller feature sizes in complex micro-nano structures. Consequently, with the design of processing strategy, phase distribution and laser processing parameters such as single-pulse energy and focused condition, a facile fabrication method for micro/nano functional devices is revealed.

2.4 Holograms devices fabricated by ultrafast laser pulses on diamond

Based on the proposed laser micropatterning method, holographic devices are fabricated on diamond substrates to modify the diffracted light field. Due to the non-uniform structure of the holographic device, it is more suitable for laser scanning processing compared to the spatial beam shaping patterning method which is better adapted for fabricating symmetric structures. Holographic devices are images created through the principles of light interference and diffraction, represent a class of optical elements. When light beam propagates through the hologram, the light field will form a specific distribution due to the effect of diffraction. Since

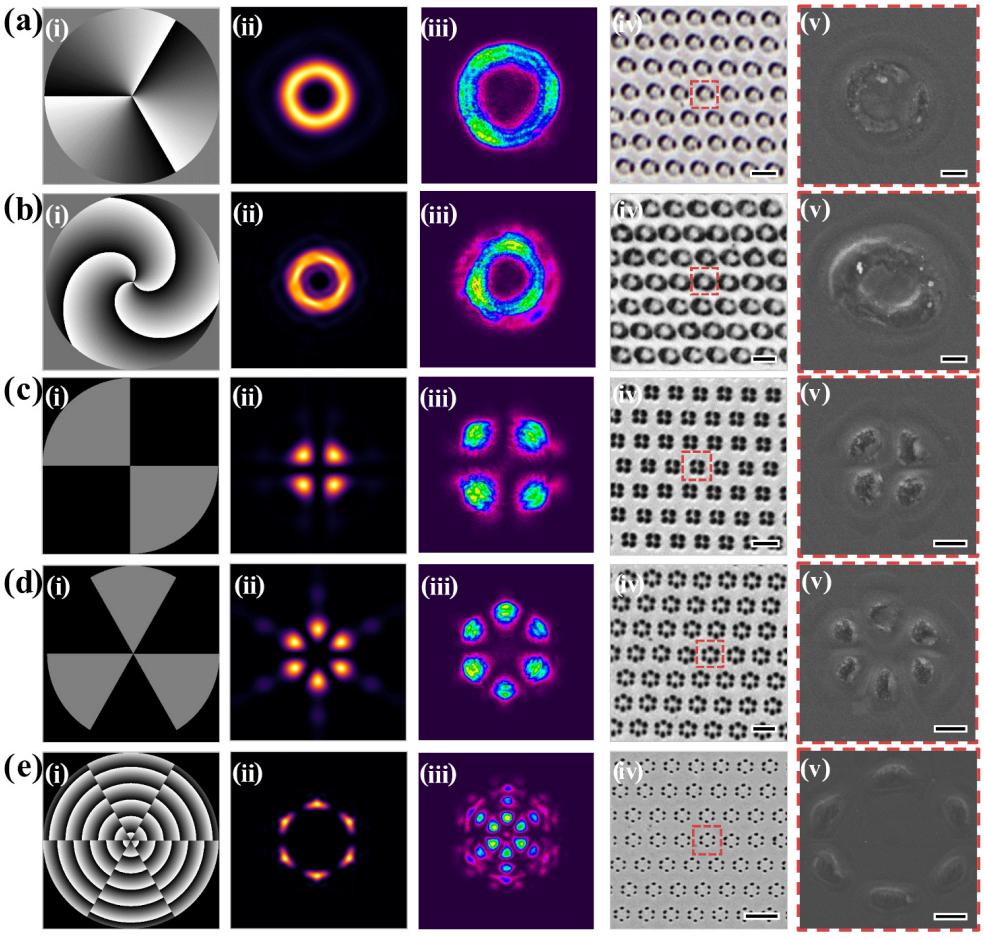

Figure 4 Design and fabrication of patterned structures using shaped laser pulse. (i) Phase holograms loaded on SLM. (a)–(e) correspond to a vortex hologram (topological charge n = 3), a Bessel hologram composed of a spiral phase plate and an axicon phase, a hologram with phase changed per 90°, a hologram with phase changed per 60°, and a hologram formed by superimposing the previous (60° step) hologram with an axicon phase, respectively. (ii) The simulated light fields corresponding to the phase in (i). (iii) The actual light fields measured in experiment. (iv) Optical images of the arrays of patterned structures, scale bar: 5 μm for (a)–(d), 10 μm for (e). (v) SEM images of single patterned structures, scale bar: 1 μm for (a)–(d), 2 μm for (e).

the diffraction pattern is mainly generated by first-order diffraction light, the diffraction efficiency has a slight impact on the practical functionality of the devices. Computed holograms could be designed via mathematical algorithms and offer possibility in generating any desired light field distribution. Based on the hologram design algorithms, we studied the application of femtosecond laser processing for fabricating computational holograms on diamonds as shown in Fig. 5.

The experimental optical path for testing the diamond-based hologram was shown in Fig. 5(a). The holographic image was reconstructed on a screen when a 530-nm wavelength laser passed through two beam lenses and an iris before illuminating the hologram. Figure 5(b) presents the original diamond target image. For processing the hologram pattern, we employed the GS algorithm, which is an iterative phase algorithm used to calculate the required phase distribution on a hologram or phase plate, to compute the phase distribution necessary to generate the target output optical field. The GS algorithm implementation proceeds as follows: A Gaussian beam is used as the incident light source, and an initial phase distribution is set on the optical diffractive device surface. Light field transmission between the incident plane and the target plane is computed iteratively using Fourier and inverse Fourier transforms. Throughout the iterations, phase information is retained, while the intensity profile is replaced with Gaussian distribution at the incident plane and the predefined distribution shown in Fig. 5(c) at the target plane, which consists of two symmetrically arranged diamond shapes. The iterative process continues until the result at the target plane sufficiently matches the desired pattern, ultimately obtaining the phase distribution on the optical diffractive device shown in Fig. 5(d), while Fig. 5(e) provides a magnified view of the calculated hologram structure. The fabrication process involved processing each pixel on the diamond substrate using single pulses with energy fluence of 526.1 J/cm^2. A laser repetition rate of 10 Hz and a scanning speed of 50 μm/s are used to ensure that each unit structure is processed by a single laser pulse. Figure 5(f) shows an optical micrograph of the resulting laser-processed hologram on the diamond surface, where dark regions indicate laser-ablated areas. The fabrication time for this holographic device was 67 min, with a measured holographic diffraction efficiency of 32.1%, which is within the theoretical diffraction efficiency range of 30%–40% for binary optical elements. A higher magnification view of this processed hologram is presented in Fig. 5(g). At the edges of the processed patterns, reduced scanning speed leads to localized over-ablation, which introduces fabrication errors. But the functionality of the holographic device is primarily determined by the overall pattern

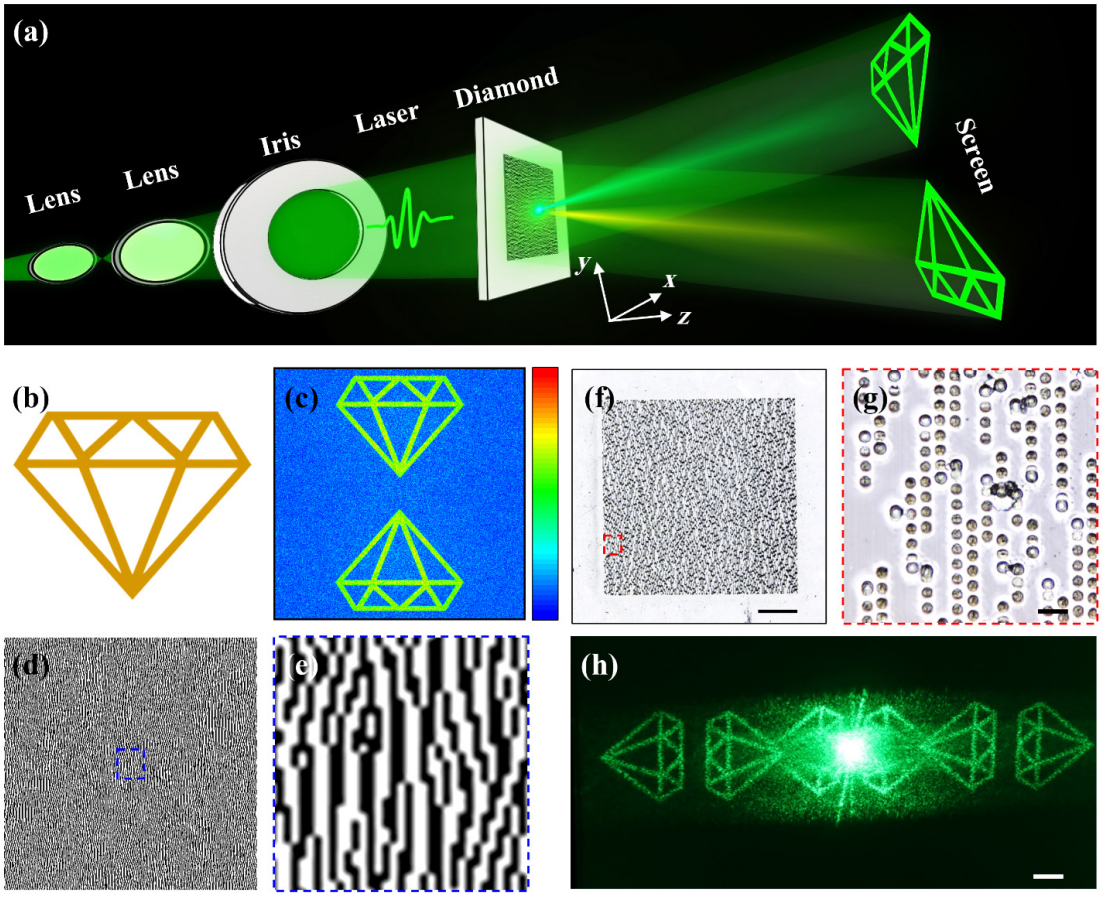

Figure 5 A holographic device processed by ultrafast laser on diamond. (a) Schematic illustration of a diamond hologram. (b) Original image, (c) simulated light field intensity distribution of the calculated hologram, (d) calculated hologram of a diamond image, and (e) a magnified view of (d). (f) Optical micrograph of the hologram fabricated on diamond surface and (g) a magnified view. (h) Measured restructured holographic images of the hologram. (f) Scale bar is 200 μm. (g) Scale bar is 10 μm. (h) Scale bar is 10 mm.

morphology and remains unaffected by localized imperfections. The functionality of the fabricated hologram was verified by projecting the reconstructed holographic image. The measurement of the diffracted light field is shown in Fig. 5(h), where multiple diamond patterns were successfully reconstructed on the screen. The generated pattern involved more than two diamond shapes, because of the effect of light diffraction.

3 Conclusions

In summary, we proposed a multimode patterning method using ultrafast laser regulated in spatial-domain to process different-scale patterns from sub-micrometer scale to millimeter scale on single-crystal diamond for functional devices fabrication. The interaction between laser pulses and single-crystal diamond was studied. It was found that, the area irradiated by laser beam performed from unprocessed, modified to ablated with the increasing of laser influence, and the degree of graphitization also increased, which provided a tunable precision for the fabrication. The free electron relaxation time of single-crystal diamond was investigated to be about 600 fs. The ablation threshold was experimentally obtained to be 36.41 J/cm^2, which was verified through simulation. Through controlling laser ablation and graphitization process, spiral patterned structures for light modulation were fabricated using point-by-point laser scanning method. By controlling the spatial energy distribution of laser beam, such as shaping the light field into four-spot light field or six-spot light field, the fabrication efficiency was improved by 3–5 times. Using the proposed laser micropatterning method, an optical diffractive device was fabricated. The holographic image of diamond was reconstructed on the screen when the fabricated device was irradiated by laser with 530-nm wavelength. To enable the fabrication of more complex and refined holographic patterns on diamond surfaces, the scanning speed of the translation stage and the complexity of the shaped light field could be considered as potential directions for improvement in the future. These advanced holographic structures would allow for precise manipulation of light propagation, and the fabricated micro-optical devices exhibit enhanced capabilities of connectivity and integration. This work demonstrates that femtosecond laser micropatterning method has broad potential applications in next-generation micro/nano functional devices, such as semiconductor-based power devices, integrated photonic systems, etc.

4 Methods

4.1 Experimental setup

A SLM-based laser direct writing system was used in the experiment. The ultrafast laser source was an amplified Ti: sapphire femtosecond laser system, with a central wavelength of 800 nm, pulse duration of 35 fs, and repetition rate of 1 kHz. The shaped

laser beams were generated by applying holograms on a 1920 × 1080 pixels liquid-crystal spatial light modulator (LC-SLM). A 4f system consisted of two convex lens was utilized to eliminate the diffraction effect before laser focusing. The focus length of convex lens was 400 mm. Then the laser was focused by an objective with a given focusing factor, like (10×, NA = 0.3), (20×, NA = 0.45), (50×, NA = 0.5), corresponding to the focal spot radius of 4.4, 2.2, and 0.88 μm respectively. The sample was positioned on a movement stage with nanoscale resolution to realize relative movement between laser beam and processed sample. The movement stage was the H-811.I2 Miniature Hexapod from Newport Corporation. Due to the high precision movement stage and the air-flotation stabilized platform, the focal plane remained stable during the entire fabrication process. A white light illumination with a Charge coupled Device (CCD) camera was used to obtain the real observation of laser direct writing process.

The diamonds used in the experiment were chemical vapor deposited (CVD) single-crystal diamonds with dimensions of either 5 mm × 5 mm or 10 mm × 10 mm, which are polished of industrial grade on both the top and bottom surfaces. The material used in processing experiment was single-crystal sample that is transparent and it is processed by Gaussian or shaped laser beam when the beam focused on the material surface. As a result, the material surface generated graphitized areas or ablated craters that were consistent with the shape of the light field.

4.2 Measurement and characterization

Optical microscope images of single-crystal diamond samples were captured under a bright-field optical microscope (Olympus). Electron microscope images of the surface structure were characterized by scanning electron microscopy (Zeiss Gemini). For the Raman spectra measurement, a continuous laser (532 nm) was used as an excitation source. Raman shift varied from 900 to 2000 cm^{-1}. The holographic image of a diamond was reconstructed on a screen after a continuous illumination laser (530 nm) traversed through two beam expansion lenses and an iris, casting light upon the hologram.

4.3 Simulation

The plasma model was employed for the simulation calculations of the processing threshold in this study. The model simulated the ultrafast laser excitation of diamond by tracking the evolution of free electron density and electron temperature. Starting from the initial laser irradiation intensity, it calculated the free electron density, electron temperature, and transient optical properties of diamond. The modified optical properties subsequently altered the laser intensity distribution at the next time step. This iterative cycle continued throughout the pulse duration, ultimately capturing the dynamic process of material ablation.

As a wide-bandgap material, the heating and collisional ionization of conduction electrons in diamond under a strong electric field can be described using the Fokker–Planck equation. After simplification and the introduction of a decay term, the equation can be expressed as

$$\frac{\mathrm{d}N(t)}{\mathrm{d}t} = a_i I(t) N(t) + R_\mathrm{p}(t) - \frac{N(t)}{\tau} \tag{1}$$

where $a_i I(t)N(t)$ corresponds to impact ionization, $R_\mathrm{p}(t)$ corresponds to photoionization, and $N(t)/\tau$ is the exponential decay term with a time constant τ.

When the diamond material becomes ionized, the localized transient optical properties undergo drastic changes, which can be represented by the following equation for free electron generation

$$\frac{\partial N(t,r,z)}{\partial t} = a_i I(t,r,z) N(t,r,z) + \delta N(I(t,r,z))^N - \frac{N(t,r,z)}{\tau} \tag{2}$$

where r is the radial distance from the beam axis, z is the depth, a_1 is the avalanche ionization coefficient, $I(t,r,z)$ is the laser intensity, δ_N is the N-photon absorption coefficient, and τ is the electron relaxation time constant. Based on double-pulse experiments, the τ for diamond has been determined to be 600 fs.

The laser input term can be assumed as a Gaussian beam profile in space and time, the laser intensity inside the diamond materials can be represented as follows

$$I(t,r,z) = \frac{2F}{\sqrt{\pi/\ln 2 t_\mathrm{p}}}(1-R(t,r))\times \exp\left(-\frac{r^2}{r_0^2} - (4\ln 2)\left(\frac{t}{t_\mathrm{p}}\right)^2 - \int_0^z \alpha(t,r,z)\mathrm{d}z\right) \tag{3}$$

where F is the laser fluence, t_p is the laser pulse duration, $R(t,r)$ is the transient reflectivity, r is distance to the laser axis, γ_0 is the beam waist, and $\alpha(t,r,z)$ is the absorption coefficient.

The optical properties of the material can be derived from the *Drude* model, which describes the transient complex dielectric function

$$\varepsilon(t,r,z) = \varepsilon_1(t,r,z) + \mathrm{i}\varepsilon_2(t,r,z) = \left(1 - \frac{\omega_\mathrm{p}^2(N)\tau_\mathrm{e}^2(t,r,z)}{1+\omega^2\tau_\mathrm{e}^2(t,r,z)}\right) + \mathrm{i}\left(\frac{\omega_\mathrm{p}^2(N)\tau_\mathrm{e}(t,r,z)}{\omega(1+\omega^2\tau_\mathrm{e}^2(t,r,z))}\right) \tag{4}$$

where $\omega_\mathrm{p}(N)$ is the plasma frequency, ω is the laser angular frequency, and τ_s is the electron relaxation time. The reflectivity $R(t,r)$ and the absorption coefficient $\alpha(t,r,z)$ can be calculated from the complex dielectric function $\varepsilon(t,r,z)$.

Through the iterative calculation of the above model and equations, the free electron density in the material under a given laser fluence can be obtained. According to the plasma model, ablation occurs when the free electron density exceeds the critical density. Therefore, the laser ablation threshold can be predicted.

Data availability

All data needed to support the conclusions in the paper are presented in the manuscript. Additional data related to this paper may be requested from the corresponding author upon request.

Acknowledgements

This work is supported by the National Key R&D Program of China (No. 2024YFB4609801), the National Natural Science Foundation of China (No. 52575510), the joint research program between Tohoku University and Tsinghua University (No. 20253080015), the Project of State Key Laboratory of Precision Manufacturing for Extreme Service Performance, Central South University (No. ZZYJKT2025-06), Beijing Natural Science Foundation (No. L255004), and High performance computing Center of Tsinghua University.

Declaration of competing interest

All the contributing authors report no conflict of interests in this work.

Author contribution statement

H. Z. H.: Conceptualization, investigation, writing – original draft, visualization. M. Q.: Conceptualization, writing – review & editing, supervision. Y. Z. Z.: Visualization. M. L.: Formal analysis. J. Q. L.: Conceptualization, investigation, writing – original draft, visualization. Y. S. Z.: Software. Y. K.: Writing – review & editing, funding acquisition. J. F. Y.: Conceptualization, writing – review & editing, supervision, funding acquisition.

Use of AI statement

None.

References

[1] Zhou, J. Y.; Su, J.; Guan, J. Y.; Yang, Y. C.; Ji, W. T.; Wang, M. Q.; Shi, F. Z.; Xia, K. W.; Wang, Y.; Du, J. F. Terabit-scale high-fidelity diamond data storage. *Nat. Photonics* **2024**, *18*, 1327–1334.

[2] Giakoumaki, A. N.; Coccia, G.; Bharadwaj, V.; Hadden, J. P.; Bennett, A. J.; Sotillo, B.; Yoshizaki, R.; Olivero, P.; Jedrkiewicz, O.; Ramponi, R. et al. Quantum technologies in diamond enabled by laser processing. *Appl. Phys. Lett.* **2022**, *120*, 020502.

[3] Atikian, H. A.; Latawiec, P.; Burek, M. J.; Sohn, Y. I.; Meesala, S.; Gravel, N.; Kouki, A. B.; Lončar, M. Freestanding nanostructures via reactive ion beam angled etching. *APL Photonics* **2017**, *2*, 051301.

[4] Cui, J. F.; Yang, Y. Y.; Yang, M. Y.; Yang, G. Y.; Chen, G. X.; Zhang, L.; Lin, C. T.; Liu, S.; Tang, C.; Ke, P. L. et al. Picometer-scale atomic shifts governing subdisordered structures in diamond. *Nano Lett.* **2024**, *24*, 7108–7115.

[5] Bütow, J.; Sharma, V.; Brandmüller, D.; Eismann, J. S.; Banzer, P. Photonic integrated processor for structured light detection and distinction. *Commun. Phys.* **2023**, *6*, 369.

[6] Chen, B.; Zhou, Y. G.; Liu, Y.; Ye, C. C.; Cao, Q.; Huang, P. N.; Kim, C.; Zheng, Y.; Oxenløwe, L. K.; Yvind, K. et al. Integrated optical vortex microcomb. *Nat. Photonics* **2024**, *18*, 625–631.

[7] Withayachumnankul, W.; Fujita, M.; Nagatsuma, T. Integrated silicon photonic crystals toward terahertz communications. *Adv. Opt. Mater.* **2018**, *6*, 1800401.

[8] Li, J. Q.; Yan, J. F.; Jiang, L.; Qu, L. T. Chiral lithography with vortex non-diffracted laser for orbital angular momentum detection. *Laser Photonics Rev.* **2024**, *18*, 2301050.

[9] Handschuh-Wang, S.; Wang, T.; Tang, Y. B. Ultrathin diamond nanofilms-development, challenges, and applications. *Small* **2021**, *17*, 2007529.

[10] Xiao, M.; Martin, I.; Yablonovitch, E.; Jiang, H. W. Electrical detection of the spin resonance of a single electron in a silicon field-effect transistor. *Nature* **2004**, *430*, 435–439.

[11] Chakrapani, V.; Angus, J. C.; Anderson, A. B.; Wolter, S. D.; Stoner, B. R.; Sumanasekera, G. U. Charge transfer equilibria between diamond and an aqueous oxygen electrochemical redox couple. *Science* **2007**, *318*, 1424–1430.

[12] Zhang, J. C.; Dong, P. F.; Dang, K.; Zhang, Y. N.; Yan, Q. L.; Xiang, H.; Su, J.; Liu, Z. H.; Si, M. W.; Gao, J. C. et al. Ultra-wide bandgap semiconductor Ga_2O_3 power diodes. *Nat. Commun.* **2022**, *13*, 3900.

[13] Gao, S.; Li, Z. Z.; Hu, Z. Y.; Yu, F.; Chen, Q. D.; Tian, Z. N.; Sun, H. B. Diamond optical vortex generator processed by ultraviolet femtosecond laser. *Opt. Lett.* **2020**, *45*, 2684–2687.

[14] Wan, N. H.; Mouradian, S.; Englund, D. Two-dimensional photonic crystal slab nanocavities on bulk single-crystal diamond. *Appl. Phys. Lett.* **2018**, *112*, 141102.

[15] Wang, H. J.; Lei, Y. H.; Wang, L.; Sakakura, M.; Yu, Y. H.; Shayeganrad, G.; Kazansky, P. G. 100-layer error-free 5D optical data storage by ultrafast laser nanostructuring in glass. *Laser Photonics Rev.* **2022**, *16*, 2100563.

[16] Li, Z. Y.; Jia, Y. W.; Duan, K.; Xiao, R.; Qiao, J. Y.; Liang, S. Y.; Wang, S. X.; Chen, J. Z.; Wu, H.; Lu, Y. et al. One-photon three-dimensional printed fused silica glass with sub-micron features. *Nat. Commun.* **2024**, *15*, 2689.

[17] Huang, P. H.; Laakso, M.; Edinger, P.; Hartwig, O.; Duesberg, G. S.; Lai, L. L.; Mayer, J.; Nyman, J.; Errando-Herranz, C.; Stemme, G. et al. Three-dimensional printing of silica glass with sub-micrometer resolution. *Nat. Commun.* **2023**, *14*, 3305.

[18] Ng, C. K.; Chen, C.; Yang, Y.; Zhang, F.; Ju, B. F.; Chen, Y. L. Femtosecond laser micro-machining of three-dimensional surface profiles on flat single crystal sapphire. *Opt. Laser Technol.* **2024**, *170*, 110205.

[19] Chen, Z.; Wei, X. B.; Lu, S. Q.; Ding, J. Q.; Du, N. Z.; Feng, C. N.; Chen, K.; Guo, P.; Lee, K. R.; Zhang, G. G. et al. Surface *in-situ* graphitization and properties of amorphous carbon film induced by laser irradiation. *Friction* **2025**, *13*, 9440977.

[20] Wang, A. D.; Das, A.; Fedorov, V. Y.; Sopeña, P.; Tzortzakis, S.; Grojo, D. In-chip critical plasma seeds for laser writing of reconfigurable silicon photonics systems. *Nat. Commun.* **2025**, *16*, 6733.

[21] Tokel, O.; Turnalı, A.; Makey, G.; Elahi, P.; Çolakoğlu, T.; Ergeçen, E.; Yavuz, Ö.; Hübner, R.; Zolfaghari Borra, M.; Pavlov, I. et al. In-chip microstructures and photonic devices fabricated by nonlinear laser lithography deep inside silicon. *Nat. Photonics* **2017**, *11*, 639–645.

[22] Xiangfu, L.; Minghui, H. Micro-cracks generation and growth manipulation by all-laser processing for low kerf-loss and high surface quality SiC slicing. *Opt. Express* **2024**, *32*, 38758–38767.

[23] Ródenas, A.; Gu, M.; Corrielli, G.; Paiè, P.; John, S.; Kar, A. K.; Osellame, R. Three-dimensional femtosecond laser nanolithography of crystals. *Nat. Photonics* **2019**, *13*, 105–109.

[24] Phillips, K. C.; Gandhi, H. H.; Mazur, E.; Sundaram, S. K. Ultrafast laser processing of materials: A review. *Adv. Opt. Photonics* **2015**, *7*, 684–712.

[25] Ali, B.; Litvinyuk, I. V.; Rybachuk, M. Femtosecond laser micromachining of diamond: Current research status, applications and challenges. *Carbon* **2021**, *179*, 209–226.

[26] Guo, H.; Xie, J. W.; He, G. Z.; Zhu, D. Z.; Qiao, M.; Yan, J. F.; Yu, J. C.; Li, J. Q.; Zhao, Y. Z.; Luo, M. et al. A review of ultrafast laser micro/nano fabrication: Material processing, surface/interface controlling, and devices fabrication. *Nano Res.* **2024**, *17*, 6212–6230.

[27] He, G. Z.; Li, J. Q.; Han, H. Z.; Yan, J. F.; Xie, J. W.; Luo, M.; Zhao, Y. Z.; Cheng, Y. H.; Qiao, M. Exploring of the effects of thermal ablation and plasma expansion on structure formation during ultrafast laser processing of Ti6Al4V alloy. *J. Mater. Process. Technol.* **2025**, *341*, 118902.

[28] Zhao, Y. Z.; Li, J. Q.; Luo, M.; Han, H. Z.; Li, Y. Y.; Xie, J. W.; Yan, J. F.; Guo, H. Ultrafast laser fabrication of a flexible sensor by selective ablation for a dynamic tactile recognition system. *ACS Appl. Mater. Interfaces* **2025**, *17*, 47130–47140.

[29] Zhao, Y. F.; Luo, M.; Hu, Y. J.; Cheng, H. H.; Yan, J. F.; Jiang, L.; Qu, L. T. Laser micro/nano fabrication of electrochemical filtering capacitors: Multiscale structural engineering for high-frequency power conditioning. *Adv. Energy Mater.* **2025**, *15*, e02620.

[30] Xie, J. W.; Yan, J. F.; Han, H. Z.; Zhao, Y. Z.; Luo, M.; Li, J. Q.; Guo, H.; Qiao, M. Photonic chip based on ultrafast laser-induced reversible phase change for convolutional neural network. *Nano-Micro Lett.* **2025**, *17*, 179.

[31] Luo, M.; Li, J. Q.; Xie, J. W.; Han, H. Z.; Yan, J. F.; Zhao, Y. Z.; Li,

Y. Y.; Cheng, H. H.; Qu, L. T. Atomic-scale ultrafast laser processing of nanocrystal with plasmonic modulation for machine learning combined flexible sensor devices. *Int. J. Extrem. Manuf.* **2026**, *8*, 025007.

[32] Dong, Y. W.; Shao, P. F.; Guo, X.; Liu, S.; Zhu, X. H.; Guo, W. Experimental study on the effect of laser overlap rate on the quality of femtosecond laser machining of micro-holes. *Opt. Laser Technol.* **2024**, *177*, 111205.

[33] Tsuru, Y.; Kozawa, Y.; Uesugi, Y.; Sato, S. Laser nanoprocessing via an enhanced longitudinal electric field of a radially polarized beam. *Opt. Lett.* **2024**, *49*, 1405–1408.

[34] Wang, X. J.; Fang, H. H.; Li, Z. Z.; Wang, D.; Sun, H. B. Laser manufacturing of spatial resolution approaching quantum limit. *Light: Sci. Appl.* **2024**, *13*, 6.

[35] Li, Z. Q.; Allegre, O.; Li, L. Realising high aspect ratio 10 nm feature size in laser materials processing in air at 800 nm wavelength in the far-field by creating a high purity longitudinal light field at focus. *Light: Sci. Appl.* **2022**, *11*, 339.

[36] Li, Z. Z.; Fan, H.; Wang, L.; Zhang, X.; Zhao, X. J.; Yu, Y. H.; Xu, Y. S.; Wang, Y.; Wang, X. J.; Juodkazis, S. et al. Super-stealth dicing of transparent solids with nanometric precision. *Nat. Photonics* **2024**, *18*, 799–808.

[37] Asgari Sabet, R.; Ishraq, A.; Saltik, A.; Bütün, M.; Tokel, O. Laser nanofabrication inside silicon with spatial beam modulation and anisotropic seeding. *Nat. Commun.* **2024**, *15*, 5786.

[38] Li, J. Q.; Yan, J. F.; Jiang, L.; Yu, J. C.; Guo, H.; Qu, L. T. Nanoscale multi-beam lithography of photonic crystals with ultrafast laser. *Light: Sci. Appl.* **2023**, *12*, 164.

[39] Ferrari, A. C.; Robertson, J. Interpretation of Raman spectra of disordered and amorphous carbon. *Phys. Rev. B* **2000**, *61*, 14095–14107.